COMMUNICATIONS

$^{31}P\{^1H\}$ NMR peak at $\delta = 34.5$ when monitored over a period of one month, showing that the Au−P bond is stable under these conditions. Crystals were transferred from hanging drops with 0.4–0.5 mm cryoloops into cryoprotectant solution (3 µL, mother liquor plus 20% glycerol), and 5 s after removal from cryoprotectant were mounted in a cryoloop (Hampton Research) and flash frozen in liquid N_2. X-ray data were collected at 100 K (Oxford Cryosystems) using MAR image plates at the Daresbury synchrotron source, and processed using DENZO. The data set consists of 185 907 measured reflections and provides a unique data set of 20 154 reflections with an $R_{merge} = 0.068$ and an overall completeness to 1.85 Å of 0.983. R_{merge} in the 1.88–1.85 Å resolution shell is 0.253.

PPIase assay: Cyp-3 was incubated with **1** at 277 K at molar ratios of **1**:Cyp-3: of 0, 0.43, 0.86, 1.0, 2.0, 3.5, 5.0, 7.0, and 10.0, for 48 h in HEPES buffer (50 mM) containing NaCl (86 mM), pH 8.0, and 4 µL aliquots were then assayed at 275 K following the procedure previously described.[12]

ESI-MS spectra of Cyp-3 after reaction with Et_3PAuCl (**1**) for five days, a colour version of Figure 3, and plots of absorbance versus time for assay of the PPIase activity of Cyp-3 are available in the Supporting Information. The atomic coordinates (code 1E3B) have been deposited in the Protein Data Bank, Research Collaboratory for Structural Bioinformatics, Rutgers University, New Brunswick, NJ (http://www.rcsb.org/).

[1] R. Bau, *J. Am. Chem. Soc.* **1998**, *120*, 9380–9381.
[2] M. T. Coffer, C. F. Shaw III, M. K. Eidsness, J. W. Watkins II, R. C. Elder, *Inorg. Chem.* **1986**, *25*, 333–339.
[3] D. T. Hill, B. M. Sutton, *Cryst. Struct. Commun.* **1980**, *9*, 679–686.
[4] C. F. Shaw III, *Chem. Rev.* **1999**, *99*, 2589–2600.
[5] M. T. Razi, G. Otiko, P. J. Sadler, *Am. Chem. Soc. Symp. Ser.* **1983**, *209*, 371–384.
[6] R. G. Pearson, *J. Am. Chem. Soc.* **1963**, *85*, 3533–3539.
[7] S. Ahrland, J. Chatt, N. R. Davies, *Q. Rev. Chem. Soc.* **1958**, *12*, 265–276.
[8] The most comprehensive database of Au sites in protein crystals is: http://www.bmm.icnet.uk/had/heavyatom.html. Most are $[Au(CN)_2]^-$ sites.
[9] Complex **1** exhibits a) antiarthritic activity: B. M. Sutton, E. McGusty, D. T. Walz, M. J. DiMartino, *J. Med. Chem.* **1972**, *15*, 1095–1098; b) anticancer activity: C. K. Mirabelli, R. K. Johnson, D. T. Hill, L. F. Faucette, G. R. Girard, G. Y. Kuo, C. M. Sung, S. T. Crooke, *J. Med. Chem.* **1986**, *29*, 218–223.
[10] Complex **1** is a major product a) from reactions of the oral drug auranofin in HCl solutions: J. Hempel, Y. Mikuriya in *Bioinorganic Chemistry of Gold Coordination Compounds* (Eds.: B. M. Sutton, R. G. Franz), SK&F, Philadelphia, **1981**, pp. 37–46; b) from reactions of auranofin with hypochlorite, an oxidant present in inflamed tissues: A. J. Canumalla, PhD thesis, University of Wisconsin-Milwaukee (USA), **1998**; c) ref. [4].
[11] A. Galat, S. M. Metcalfe, *Prog. Biophys. Mol. Biol.* **1995**, *63*, 67–118.
[12] J. Dornan, A. P. Page, P. Taylor, S.-Y. Wu, A. D. Winter, H. Husi, M. D. Walkinshaw, *J. Biol. Chem.* **1999**, *274*, 34877–34883. Cyp-3 (173 amino acids) has a high sequence and structural similarity to human Cyp-A.
[13] The expressed protein lacks Met1.
[14] G. M. Sheldrick, **1997**, SHELXL-97, University of Göttingen, Germany.
[15] B. Bovio, F. Bonati, A. Burini, B. R. Pietroni, *Z. Naturforsch.* **1984**, *39B*, 1747–1754.
[16] S. J. Berners-Price, M. J. Dimartino, D. T. Hill, R. Kuroda, M. A. Mazid, P. J. Sadler, *Inorg. Chem.* **1985**, *24*, 3425–3434.
[17] J. L. Kofron, P. Kuzmic, V. Kishore, E. Colonbonilla, D. H. Rich, *Biochemistry* **1991**, *30*, 6127–6134.
[18] J. Liu, C. T. Walsh, *Proc. Natl. Acad. Sci. USA* **1990**, *87*, 4028–4032.
[19] J. Strähle in *Gold: Progress in Chemistry, Biochemistry and Technology* (Ed.: H. Schmidbaur), Wiley, Chichester, **1999**, pp. 311–348.
[20] a) M. T. Razi, PhD thesis, University of London, **1983**; b) M. T. Razi, P. J. Sadler, unpublished results. ^{35}Cl NMR studies show that one molar equivalent of L-Cys is sufficient to displace all the bound Cl^- ions from **1**, whereas more than eight molar equivalents of N-methylimidazole are required.
[21] N. A. Malik, G. Otiko, P. J. Sadler, *J. Inorg. Biochem.* **1980**, *12*, 317–322.
[22] C. F. Shaw III, N. A. Schaeffer, R. C. Elder, M. K. Eidsness, J. M. Trooster, G. H. M. Calis, *J. Am. Chem. Soc.* **1984**, *106*, 3511–3521.
[23] a) G. Otiko, P. J. Sadler, *FEBS Lett.* **1980**, *116*, 227–30; b) M. C. Grootveld, G. Otiko, P. J. Sadler, R. Cammack, *J. Inorg. Biochem.* **1986**, *27*, 1–15.
[24] A. F. S. A. Habeeb, *Methods Enzymol.* **1972**, *25*, 457–464.
[25] P. C. Jocelyn, *Methods Enzymol.* **1987**, *143*, 44–67.
[26] R. M. Esnouf, *J. Mol. Graphics Modelling* **1997**, *15*, 132–136.
[27] P. J. Kraulis, *J. Appl. Crystallogr.* **1991**, *24*, 946–950.
[28] E. A. Merritt, D. J. Bacon, *Methods Enzymol.* **1997**, *277*, 505–524.

DeNO*x* of Exhaust Gas from Lean-Burn Engines through Reversible Adsorption of N_2O_3 in Alkali Metal Cation Exchanged Faujasite-Type Zeolites**

Asima Sultana, Raf Loenders, Orietta Monticelli, Christine Kirschhock, Pierre A. Jacobs, and Johan A. Martens*

Nitrogen oxide (NO_x) adsorbents are key control components for the tailpipe emissions of transport vehicles powered with lean-burn engines. Current adsorbents are basic oxides which adsorb NO_x as nitrates, but suffer from poisoning by sulfur oxides. We discovered that NO and NO_2 can be selectively trapped as dinitrogen trioxide in alkali metal exchanged faujasite zeolites above 200 °C. The trapped N_2O_3 molecules compete with water molecules on a specific adsorption site and can be displaced by a change in partial pressure. Dinitrogen trioxide adsorption is not affected by the presence of sulfur oxides.

Modern lean-burn internal combustion engines operated with excess air show reduced fuel consumption and carbon dioxide emission but produce excessive amounts of nitrogen oxides (NO_x). The emission of NO_x at the tailpipe is the major source of pollution from transport vehicles powered by hydrocarbon fuels.[1] Since there is a trade-off between NO_x and particulate carbon formation in the lean-burn engine, an efficient NO_x-elimination system for the exhaust can offer a solution to the particulate carbon emissions at the same time.[2] In the emerging technologies that focus on reducing the NO_x emission from lean-burn engines, temporary storage

[*] Prof. Dr. ir. J. A. Martens, Dr. A. Sultana, Dr. R. Loenders,
Dr. O. Monticelli, Dr. C. Kirschhock, Prof. Dr. ir. P. A. Jacobs
Centrum voor Oppervlaktechemie en Katalyse
Katholieke Universiteit Leuven
Kardinaal Mercierlaan 92, 3001 Heverlee (Belgium)
Fax: (+32) 16-321998
E-mail: johan.martens@agr.kuleuven.ac.be

Supporting information for this article is available on the WWW under http://www.wiley-vch.de/home/angewandte/ or from the author.

of NO$_x$ molecules on an adsorbent is a key step. In a NO$_x$-storage-and-reduction catalytic system,[3] an oxidation catalyst that converts nitric oxide into nitrates is combined with basic oxides that are responsible for nitrate chemisorption. Periodically the nitrates are reduced in the rich exhaust gas produced by the engine. In the selective-NO$_x$-recirculation technique,[4] trapped NO$_x$ is periodically desorbed and reinjected into the engine. The drawback of nitrate adsorbents is that they are gradually deactivated by the accumulation of the more stable sulfates that originate from the combustion of fuel containing organic sulfur.

Dinitrogen trioxide can be formed in *dry* zeolites upon exposure to nitric oxide,[5] to nitric oxide and oxygen,[6, 7] or to mixtures of nitrogen dioxide and nitric oxide.[6] In *dry* zeolites the dinitrogen trioxide molecule undergoes heterolytic splitting into a nitrosonium cation and a nitrite and/or nitrate anion,[7, 8] or reacts with Brønsted acid sites to form a nitrosonium cation and water, as evidenced by IR spectroscopy.[9] With real exhaust gas, which always contains water, the NO$_x$ chemistry is different.[5, 9, 10] In alkali or alkaline earth metal exchanged zeolite Y, nitrogen dioxide reacts with water at $80\,°C$ to form nitrate with release of nitric oxide [Eq. (1); M^{n+} represents the valent charge compensating cation, and Z^- the negatively charged zeolite lattice]. The zeolite shows no affinity for NO at this temperature in the presence of water vapour.[10]

$$3n\,NO_2 + n\,H_2O + 2[M^{n+}(Z^-)_n] \longrightarrow 2M(NO_3)_n + n\,NO + 2n\,H\text{-}Z \qquad (1)$$
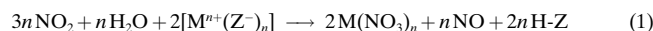
A representative mixture of oxidized exhaust gas composed of helium with 500 ppm NO, 500 ppm NO$_2$, 5% water, 10% O$_2$, and 5% CO$_2$ was conducted over a bed of Na-Y zeolite at $150\,°C$ (Figure 1A). The change in the NO and NO$_2$ concentrations between the inlet and outlet (Figure 1A) reveal a temporary complete adsorption of the NO$_2$ and a simultaneous formation of nitric oxide, the quantity of which corresponds to about one third of the adsorbed NO$_2$ [Eq. (1)].

A similar experiment performed at $250\,°C$ (Figure 1B) reveals totally different adsorption chemistry. At this temperature NO and NO$_2$ are simultaneously adsorbed for a few minutes. The formation of N$_2$O$_3$ in the zeolite under these conditions was revealed by a Rietveld refinement in combination with Fourier analysis of the X-ray diffraction powder pattern (Figure 2). N$_2$O$_3$ molecules were shown to be localized at a unique position in the supercage of zeolite Y (Figure 2A and B). Under these conditions the supercages are filled with networks of water molecules that link sodium ions at the SIII positions with sodium ions SII and SV.[11] The refined geometry of the N$_2$O$_3$ molecule (Figure 2C) is very close to the most stable asymmetric conformer.[12] By assuming this position in the zeolite Na-Y the three oxygen atoms of an N$_2$O$_3$ molecule substitute three oxygen atoms of water molecules in the sodium–water net. Oxygen atom On1 bridges an SIII and an SV sodium ion, while the two On2 oxygen atoms are coordinated to the same SIII sodium ion and an SII sodium ion (Figure 2C).

If a homogeneous distribution of the sodium ions and water molecules over the hydrated Na-Y crystals prior to NO$_x$
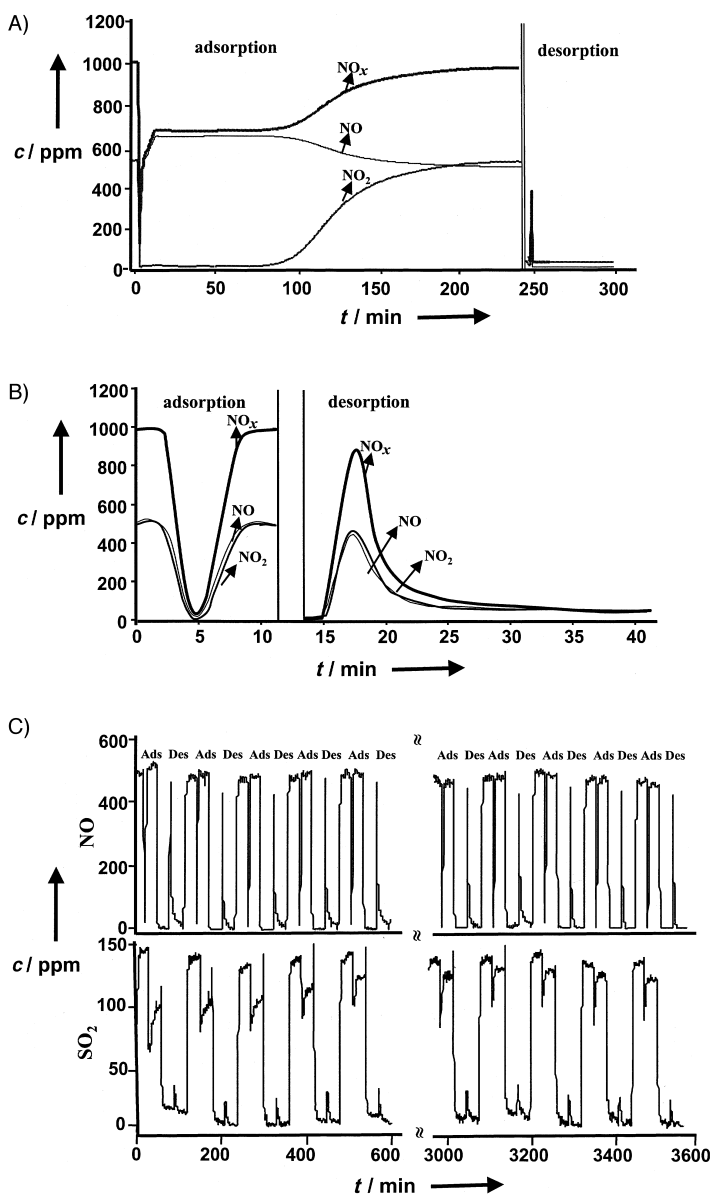

Figure 1. NO$_x$, NO$_2$, NO, and SO$_2$ concentration changes in the outlet of the Na-Y adsorbent bed during NO$_x$ adsorption and desorption at $150\,°C$ (A) and $250\,°C$ without and with SO$_2$ (B and C, respectively). Adsorption conditions: helium with 500 ppm NO, 500 ppm NO$_2$, 5% CO$_2$, 5% H$_2$O, 10% O$_2$, and 150 ppm SO$_2$ (in C); VHSV = 30000 h^{-1}. Desorption conditions: helium containing 5% H$_2$O; VHSV = 15000 h^{-1}.

adsorption is assumed, then each supercage contains at least one SV sodium cation together with SII and SIII sodium ions, and offers at least one adsorption site for N$_2$O$_3$. The fraction of supercages holding an N$_2$O$_3$ molecule in the saturated Na-Y sample was 0.15 according to the refined occupancy factors (see the supporting information) and 0.12 according to the NO and NO$_2$ uptake derived from the inlet and outlet concentration profiles (Figure 1B). The partial saturation of the adsorption sites reflects the competition between the adsorption of N$_2$O$_3$ molecules and three water molecules [Eq. (2)].

$$Na_x(H_2O)_y + NO + NO_2 \rightleftharpoons Na_x(H_2O)_{y-3}(N_2O_3) + 3H_2O \qquad (2)$$
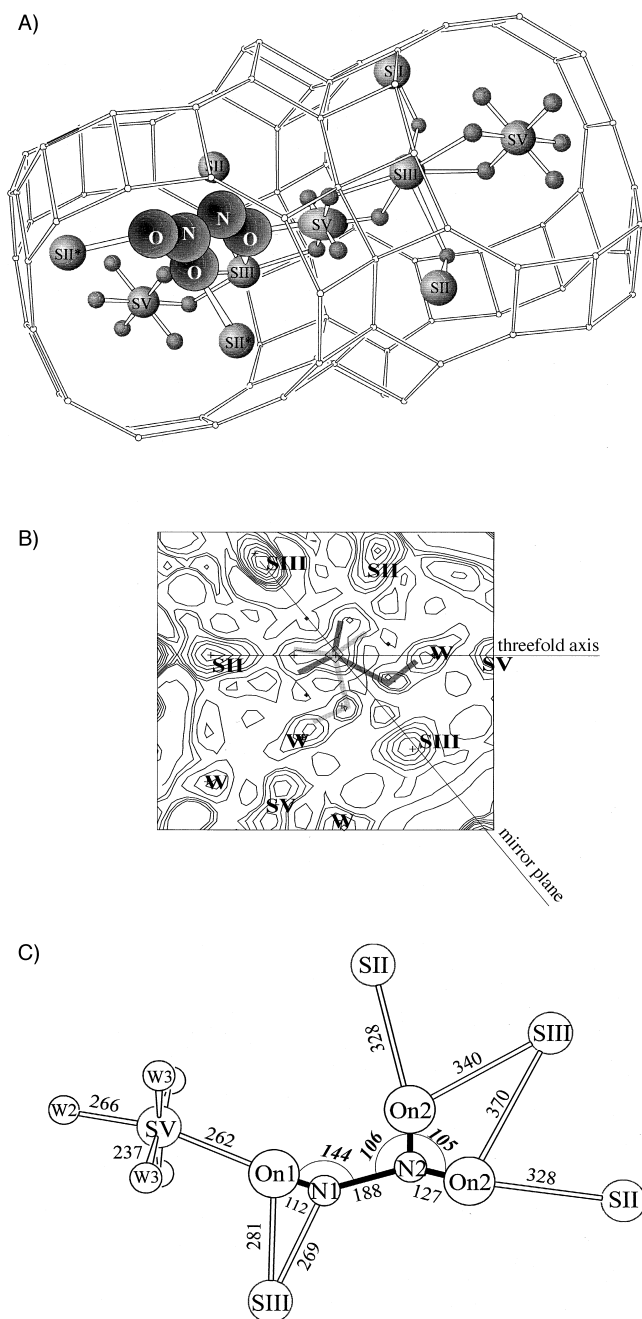
A)

B)

C)
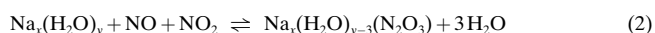
Figure 2. A) Rietveld-refined position of N_2O_3 (largest spheres), water (small spheres), and sodium cations (medium size spheres) in zeolite Na-Y (the lines in the ball and stick representation of the zeolite show the TO_2 tetrahedra of the framework; oxygen atoms are found between the Si or Al atoms). B) Observed electron density map revealing two symmetrically equivalent positions for the N_2O_3 molecule. C) Detailed representation of the N_2O_3 molecule and adjacent sodium ions. Bond lengths [pm] and angles [°] are indicated.

N_2O_3 can be desorbed as NO and NO_2 by displacing the equilibrium in Equation (2) by flushing the adsorbent bed with water-containing gas (Figure 1 B). In contrast to this, the nitrate-saturated zeolite Na-Y can not be regenerated with hydrated helium gas (Figure 1 A).

The formation of dinitrogen trioxide at 260 °C was monitored by FT-IR spectroscopy (Figure 3 A). IR absorption bands were observed around 1270, 1590, and 1905 cm^{-1} in an
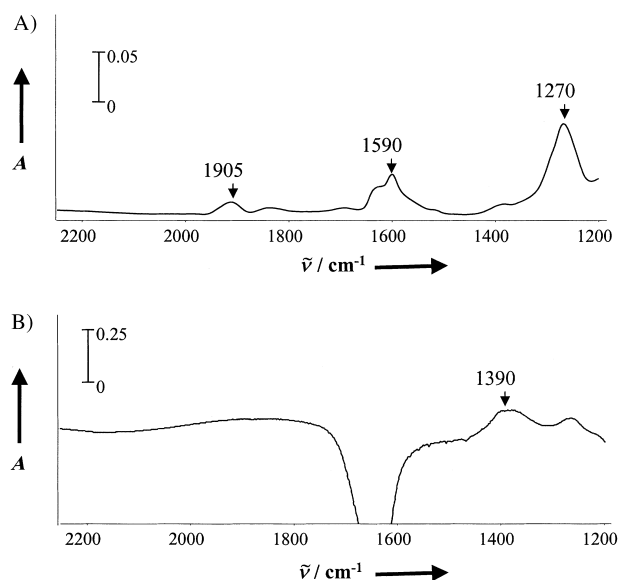
A)

B)

Figure 3. FT-IR difference spectra A) of Na-Y saturated with N_2O_3 at 260 °C and after evacuation of the cell with wet helium and B) of Na-Y saturated with nitrate obtained by cooling the N_2O_3 saturated Na-Y sample 40 °C with fresh hydrated Na-Y sample. A = absorption.

N_2O_3-saturated sample, which were assigned to the nitro symmetric stretch, nitro asymmetric stretch, and nitroso stretch, respectively, of the asymmetric N_2O_3 conformer.[7, 9, 12–14] The signals disappear upon evacuation of the sample with hydrated helium gas. Cooling the N_2O_3-saturated sample to 40 °C leads to an IR absorption band around 1390 cm^{-1} (Figure 3 B), which is assigned to nitrate.[10]

The temperature dependence of the nitrate and dinitrogen trioxide adsorption capacity, derived from the NO and NO_2 uptake curves, is shown in Figure 4. Nitrate formation diminishes with increasing temperature and vanishes above 300 °C. The N_2O_3 adsorption capacity peaks at 250 °C.
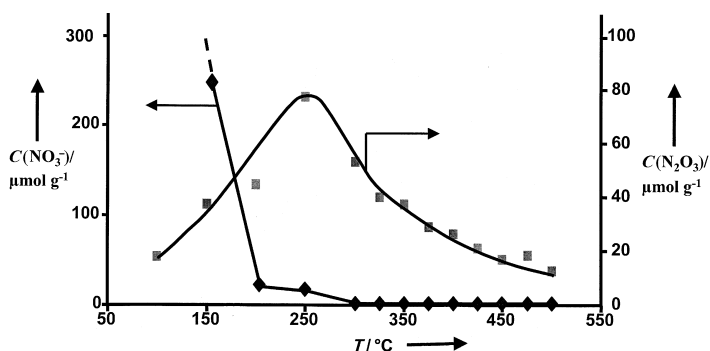

Figure 4. Temperature dependence of the nitrate and dinitrogen trioxide adsorption capacity C of zeolite Na-Y.

Experiments carried out at 250 °C with synthetic exhaust gas containing more NO_2 than NO showed that NO_2 can be adsorbed in molar quantities exceeding those of NO. Inspection of the adsorption site of N_2O_3 (Figure 2 A and B) reveals that the adsorption of N_2O_4 can occur on the same site as N_2O_3. The preferential formation of N_2O_3 from equimolar mixtures of NO and NO_2 is explained by the higher stability of

N_2O_3 relative to N_2O_4[15] and the much faster association kinetics.[16]

An Na-Y sample was subjected to successive isothermal adsorption–desorption cycles at 250 °C for three days using synthetic exhaust gas spiked with 150 ppm SO_2. Regeneration of the sample was achieved with hydrated helium gas (Figure 1 C). In the 30 cycles made the N_2O_3 adsorption capacity remained constant at (77 ± 6) μmol g^{-1}, which corresponds to the capacity measured in absence of SO_2. The low uptake of SO_2 in the first cycles decreased with operation time (Figure 1 C). In experiments to test for the control of NO_x emission, this N_2O_3 adsorbent shows high sulfur resistance. Furthermore, it allows the use of regeneration through a change of partial pressure in a water-containing gas such as hydrated air and does not necessitate heating.

Zeolites with the faujasite (FAU) framework topology can exist in different chemical compositions. For reasons of charge balance, the molar sodium content of the zeolite must equal the molar aluminum content in the framework. The formation of the water–sodium clusters that are active in N_2O_3 adsorption requires specific occupations of SII, SIII, and SV sites with sodium (Figure 2) and depends on the Si/Al atomic ratio of the faujasite framework. If the occupancies of these sites in Na-X (Si/Al = 1.2) and Na-Y (Si/Al = 1.7) zeolites are too high, nitrate adsorption is favored irrespective of temperature. The highest adsorption capacity for N_2O_3 was encountered in commercial Na-Y samples with Si/Al atomic ratios ranging from 2.4 to 2.6. Siliceous Na-Y zeolites such as EMC-1 (Si/Al = 3.6)[17] have a decreased N_2O_3 capacity of 47 μmol of N_2O_3 per gram at 250 °C. This result is a direct consequence of the lower number of sodium ions available to form SII-SIII-SV water nets. Moreover, the screening of zeolite samples showed that N_2O_3 adsorption is unique to Y zeolites with FAU topology. Even the closely related EMC-2 zeolite (Si/Al = 3.7; EMT topology)[17] did not show appreciable N_2O_3 adsorption.

Experimental Section

The NO and NO_2 concentrations in the NO_x adsorption experiments were monitored with a chemiluminescence detector (Eco Physics, CLD 700 EL ht). N_2O was analyzed on a ND-IR spectrophotometer (Maihak, Unor 610). A bed of compressed zeolite powder with particle size of 0.3–0.50 mm was mounted in a quartz tube of 0.9 mm internal diameter that fitted in a tubular furnace. He, O_2, CO_2, SO_2, NO, and NO_2 were fed from gas cylinders using mass flow controllers. A stream of water-saturated helium gas was added after mixing all the other gases. The experiments depicted in Figure 1 were performed on 400 mg of Na-Y zeolite (Si/Al atomic ratio = 2.6, Zeolyst), which represents a bed volume of 0.6 mL. The adsorber was first by-passed for a few minutes to verify the inlet NO_x levels. The gas was then allowed to flow through the adsorbent bed at 300 mL min^{-1} (standard conditions), which corresponds to a volumetric hourly space velocity (VHVS) of 30 000 h^{-1}. After saturation of the adsorbent, identified by a NO_x level reaching the inlet value, the adsorber was closed, the lines flushed with the desorption gas, and the adsorbent bed evacuated while monitoring the NO_x concentration.

The FT-IR spectra were recorded using a Nicolet 730 instrument equipped with a cell with CaF_2 windows holding a Na-Y zeolite wafer with a density of 5 mg cm^{-2}. The spectral resolution was 2 cm^{-1} and the number of scans 500. The sample was heated to 260 °C in a wet helium atmosphere, exposed to helium gas containing 500 ppm NO, 500 ppm NO_2, and 5% water, and evacuated with hydrated helium gas (Figure 3 A). In another experiment (Figure 3 B) the sample was cooled to 40 °C after exposure to the NO_x-containing gas at 260 °C.

The position and nature of the adsorbed NO_x species were determined from a comparative Rietveld study of the X-ray powder patterns of the Na-Y sample contacted with hydrated helium gas (5% water) and with a gas mixture composed of 500 ppm NO, 500 ppm NO_2, 5% CO_2, 5% H_2O, and 10% O_2 at 250 °C. XRD patterns of samples in sealed capillaries (internal diameter: 0.5 mm) were recorded at room temperature in a Debye Scherrer geometry on a Stadi P diffractometer with Cu$_{K\alpha1}$ radiation. Both samples were also measured at 250 °C between $2\theta = 4-35°$ and no changes in the intensity of the Bragg reflections at room temperature and 250 °C were detected. The arrangement of water molecules and sodium ions in the host are not dependent on temperature, but on the amount of water present in the cavities.[11] Refinement was conducted on data sets between $2\theta = 4-70°$. The low angle region was simultaneously refined with a different set of profile parameters. The GSAS software package was used to analyze the data. Structural parameters were refined starting with the data for a sample hydrated at 200 °C.[11] This cation–water arrangement described the sample used for NO_x adsorption correctly. Only small changes in the powder pattern were observed after the adsorption of NO_x. An analysis of the observed and difference electron density allowed the NO_x molecules positions to be determined, which were identified by comparison with the asymmetric N_2O_3 conformer (Figure 2). Initially the molecules were introduced as rigid bodies into the Rietveld refinement. Towards the end of the refinement the rigid-body constraints were dropped. The occupancy factors within the molecule were constricted to represent the molecular formula. Thermal parameters of the molecule were kept fixed. The refined powder pattern and the refined parameters of Na-Y holding N_2O_3 are given in the Supporting Information.

[1] R. A. Searles, *Stud. Surf. Sci. Catal.* **1998**, *116*, 23–33.

[2] P. L. Herzog, *Stud. Surf. Sci. Catal.* **1998**, *116*, 35–48.

[3] K. Kato, T. Inoue, H. Nohira, K. Nakanishi, S. Iguchi, T. Kihara, H. Muraki (Toyota), EU-B 0573 672 A1, **1993**.

[4] B. Krutzsch, G. Wenninger, M. Weibel, P. Stapf, A. Funk, D. E. Webster, E. Chaize, B. Kasemo, J. Martens, A. Kiennemann, *SAE Prepr.* **1998**, 982592, 1–9.

[5] W. E. Addison, R. M. Barrer, *J. Chem. Soc.* **1955**, 757–769.

[6] B. J. Adelman, G. D. Lei, W. M. H. Sachtler, *Catal. Lett.* **1994**, *28*, 119–130.

[7] E. Ito, Y. J. Mergler, B. E. Nieuwenhuys, H. van Bekkum, C. M. van den Bleek, *Microporous Mater.* **1995**, *4*, 455–465.

[8] P. H. Kasai, R. J. Bishop, *J. Am. Chem. Soc.* **1972**, *94*, 5560–5566.

[9] K. Hadjiivanov, J. Saussey, J. L. Freysz, J. C. Lavalley, *Catal. Lett.* **1998**, *52*, 103–108.

[10] O. Monticelli, R. Loenders, P. A. Jacobs, J. A. Martens, *Appl. Catal. B* **1999**, *21*, 215–220.

[11] C. E. A. Kirschhock, B. Hunger, J. A. Martens, P. A. Jacobs, *J. Phys. Chem. B* **2000**, *104*, 439–448.

[12] C. H. Bibart, G. E. Ewing, *J. Chem. Phys.* **1974**, *61*, 1293–1299.

[13] J. Szanyi, M. T. Paffett, *J. Catal.* **1996**, *164*, 232–245.

[14] K. Hadjiivanov, L. Dimitrov, *Microporous Mesoporous Mater.* **1999**, *27*, 49–56.

[15] B. Markwalder, P. Gozel, H. van den Bergh, *J. Phys. Chem.* **1993**, *97*, 5260–5265.

[16] I. W. M. Smith, G. Yarwood, *Chem. Phys. Lett.* **1986**, *130*, 24–28.

[17] F. Delprato, L. Delmotte, J.-L. Guth, L. Huve, *Zeolites* **1990**, *10*, 546–552.